NASA Technical Memorandum 107321

Critique of Macro Flow/Damage Surface Representations for Metal Matrix Composites Using Micromechanics

Cliff J. Lissenden
Pennsylvania State University
University Park, Pennsylvania

and

Steven M. Arnold
Lewis Research Center
Cleveland, Ohio

National Aeronautics and
Space Administration

CRITIQUE OF MACRO FLOW/DAMAGE SURFACE REPRESENTATIONS FOR METAL MATRIX COMPOSITES USING MICROMECHANICS

Cliff J. Lissenden
Department of Engineering Science and Mechanics
Penn State University
University Park, PA 16802

Steven M. Arnold
Structural Fatigue Branch
NASA Lewis Research Center
Cleveland, OH 44135

ABSTRACT

Guidance for the formulation of robust, multiaxial, constitutive models for advanced materials is provided by addressing theoretical and experimental issues using micromechanics. The multiaxial response of metal matrix composites, depicted in terms of macro flow/damage surfaces, is predicted at room and elevated temperatures using an analytical micromechanical model that includes viscoplastic matrix response as well as fiber-matrix debonding. Macro flow/damage surfaces (i.e., debonding envelopes, matrix threshold surfaces, macro "yield" surfaces, surfaces of constant inelastic strain rate, and surfaces of constant dissipation rate) are determined for silicon carbide/titanium in three stress spaces. Residual stresses are shown to offset the centers of the flow/damage surfaces from the origin and their shape is significantly altered by debonding. The results indicate which type of flow/damage surfaces should be characterized and what loadings applied to provide the most meaningful experimental data for guiding theoretical model development and verification.

INTRODUCTION/BACKGROUND

Aerospace structural components are commonly subjected to thermomechanical service conditions, involving multiple temperature levels, thermal transients and mechanical loads, severe enough to result in significant nonlinear (e.g., inelastic or damage induced) deformation. The accurate prediction of the stress, strain and temperature fields within these structural components depends strongly upon accurate mathematical representations (constitutive equations) of the nonlinear behavior of structural materials (e.g., monolithic alloys or advanced composite systems) at high temperature. To be generally applicable, these constitutive equations must be expressed in multiaxial form and be appropriate for all anticipated modes of mechanical and thermal loading (e.g., cyclic, nonisothermal, nonproportional, etc.). This is an imposing task, nevertheless significant advancement has been achieved over the past two decades with the

advent of unified viscoplastic constitutive models (e.g., Walker (1981), Bodner (1987), Helling and Miller (1987), Robinson and Duffy (1990), Freed and Walker (1995), Arnold et al. (1996a,b)). Historically, with the exception of Spencer (1972), uniaxial constitutive response has been the focal point of research on anisotropic materials. Recently, attention has being focused on describing the multiaxial constitutive behavior (e.g., Robinson and Duffy (1990), and Saleeb and Wilt (1993)), for new generations of advanced structural materials that possess strong directional characteristics (e.g., directionally solidified metals, metal and intermetallic matrix composites as well as ceramic and polymeric composites). Such advanced materials offer the designer the additional advantage of tailoring his design to have increased strength, stiffness, conductivity and the like in one or more preferred directions.   Under high temperature thermomechanical service conditions these advanced materials still exhibit all the time-dependent hereditary behavior of more conventional alloys but now their directional nature adds yet another level of complexity. Consequently, the further development and validation of multiaxial viscoplastic models for metal matrix composites is essential if these advanced materials are to be utilized by the aerospace and power generation industries.

A key ingredient in the formulation of robust, multiaxial, constitutive models is the close interaction between experimentalists and theoreticians in establishing the required developmental program. Three types of experimentation (Robinson (1985)) are necessary to support the rational formulation of constitutive models for high temperature structural material systems (be they monolithic or composite). These are 1) Exploratory tests that guide the development and examine the fundamental concepts and mathematical constructs embedded in the theoretical framework, 2) Characterization tests that provide the required data base for determining the specific functional forms and material parameters to represent a particular material over a given range of conditions, and 3) Verification tests, (often prototypical in nature) that provide the ultimate test of a constitutive model through comparison of actual structural component response with analytical predictions based on a given model. As results from these tests should ideally provide feedback for subsequent developmental efforts, the best verification tests may be those of simple structures such as beams, plates, shells and bar structures under prototypical conditions of temperature, stress, strain-rate, etc.

The present work will primarily focus upon practical and theoretical issues relative to conducting and analyzing tests of the exploration type, i.e., determination of multiaxial flow/damage surfaces for titanium matrix composites (TMCs). However, it is important to realize that such exploratory tests on composite materials (which are actually structures) can in themselves be viewed as verification tests (for both the constitutive model and homogenization (micromechanics) technique), provided the constitutive equations being verified are developed utilizing only constituent material properties. This distinction will be developed further within the body of the report. The necessity of conducting such fundamental multiaxial flow/damage surface tests can be best understood in the context of classical plasticity; in as much as the concept of a yield surface plays a central role in that it delineates the elastic and inelastic deformation regions of the material. The existence and description of this yield surface is precisely that which allows a consistent multiaxial statement of plastic flow (flow law) to be written. Mathematically, this is done by making use of the fundamental assumption that the yield surface has the properties of a potential (normality), e.g.

$$f\left(\sigma_{ij}, \alpha_{ij}, T\right) = k$$

and thus leads to an associated form of the flow law through differentiation of f, that is

$$d\varepsilon_{ij}^{i} = \frac{\partial f}{\partial \sigma_{ij}}$$

where, $\sigma_{ij}, \alpha_{ij}, \varepsilon_{ij}^{i}, T,$ and k are the applied Cauchy stress, back (internal) stress and inelastic strain tensors, temperature and yield stress, respectively.

Experimentally, yield surfaces are typically mapped out using an equivalent inelastic strain definition and a rather arbitrary target value of permanent set. The impact of the magnitude of this target value will be indicated subsequently. Multiaxial testing alone provides a quantitative description of f, thereby allowing a correct mathematical form of the flow law to be deduced. To date significant testing has been done in support of the concept of a yield surface and the normality condition, albeit at relatively low temperatures and for monolithic materials (e.g. Phillips (1974), Liu and Greenstreet (1976), Ellis et al. (1978) and Oytana et al. (1982)). Note, as we are concerned here with primarily examining composite materials, "yield" will be defined to have occurred whenever deviation from proportionality (DFP) has been exceeded by a specified target value. In this way the inelastic response can encompass both matrix inelasticity and internal damage resulting from fiber-matrix debonding.

At elevated temperatures, metallic alloys and TMCs typically exhibit strong time-dependent deformation behavior and the concept of a yield surface, in the classical sense, generally breaks down as we move into the realm of viscoplasticity. However, analogous geometrical and thermodynamically based concepts such as surfaces of constant inelastic strain rate (SCISRs) and surfaces of constant dissipation rate (SCDRs)[1] can and have been postulated to play the same central role in viscoplastic constitutive theories as yield surfaces do in classical plasticity. In fact, given a complete (i.e., fully associative) potential based framework, as that proposed by Arnold and Saleeb (1994), the experimental multiaxial identification of the Gibbs and dissipation potential would completely define the ensuing compliance operator and flow and evolution laws for the inelastic strain and internal state variables, respectively. This fundamental approach to the formulation of a consistent multiaxial theory is in stark contrast to the more typical ad hoc and generally inadequate approach of extending uniaxial constitutive theories for multiaxial conditions by simply placing bars over the pertinent variables and declaring them "effective" values. This systematic approach becomes even more important when one deals with materials that have preferred directions (e.g. TMCs), as the anisotropy and potential for internal damage (i.e., since debonding is prevalent in TMCs, where it can occur prior to plastic flow in the matrix) further complicates the shapes of these surfaces in various stress spaces. Many researchers have documented the effects of debonding on the overall deformation response of TMCs (e.g., Johnson et al. (1990), Jansson et al. (1991), Majumdar and Newaz (1992), Lerch and Saltsman (1993), Lissenden et al. (1996a)).

Both of the above definitions (i.e., for SICSRs see Battiste and Ball (1986) and for SCDRs see Clinard and Lacombe (1988)) have been used to describe the form of the dissipation potential at elevated temperatures for monolithic materials. However, the utility (both theoretically and experimentally) of using a SCISR or SCDR concept to define the requisite state dependence of

---

[1] SCDRs are defined to be $\Sigma_{ij}\dot{\varepsilon}_{ij}^{i}$, where Σ_{ij} is the effective deviatoric stress tensor (i.e., $\Sigma_{ij} = s_{ij} - a_{ij}$, with s_{ij} being the applied (external) deviatoric stress and a_{ij} the back (internal) deviatoric stress) and $\dot{\varepsilon}_{ij}^{i}$ the inelastic strain rate tensor; and SCISRs are defined as $\dot{\varepsilon}_{ij}^{i}\dot{\varepsilon}_{ij}^{i}$.

3

the dissipation potential requires careful consideration as these "definitions" may or may not be equivalent, particularly with regard to quantifying the multiaxial behavior of anisotropic materials. To substantiate this statement, let us first consider an isotropic, monolithic, material having a dissipation potential $\Omega(F,G)$ that depends on the external stress through the scalar function F and on the internal variables (the back stress in this case) through the scalar function G (Robinson and Ellis (1986) and Hopkins (1990)). From normality, the flow law becomes,

$$\dot{\varepsilon}_{ij}^{i} = \frac{\partial\Omega}{\partial\sigma_{ij}} = \frac{\partial\Omega}{\partial F}\frac{\partial F}{\partial\sigma_{ij}}. \tag{1}$$

If F and $\dfrac{\partial\Omega}{\partial F}$ are prescribed to be

$$F = \frac{\left(J_2^3 + cJ_3^2\right)^{\frac{1}{3}}}{k^2} - 1, \quad \frac{\partial\Omega}{\partial F} = f^*(F), \tag{2}$$

where $J_2 = \dfrac{1}{2}\Sigma_{ij}\Sigma_{ij}$ and $J_3 = \dfrac{1}{3}\Sigma_{ij}\Sigma_{jk}\Sigma_{ki}$ are the second and third invariants of the effective deviatoric stress, respectively, c is a constant, and $f'(F)$ is an unspecified function, then for a fixed inelastic state, i.e. G=constant ≈ 0,

$$\Sigma_{ij}\dot{\varepsilon}_{ij}^{i} = 2f^*(F)k^2(F+1)$$

$$\dot{\varepsilon}_{ij}^{i}\dot{\varepsilon}_{ij}^{i} = \frac{2f^{*2}(F)}{k^6(F+1)^2}\left\{\left[(F+1) + \frac{cJ_3^2}{k^6(F+1)^2}\left(1 - \frac{8}{27}c\right)\right]J_2^2 + \frac{2c^2J_3^2}{k^6(F+1)^2}J_4\right\}, \tag{3}$$

where $J_4 = \dfrac{1}{9}\Sigma_{ik}\Sigma_{kj}\Sigma_{il}\Sigma_{lj}$. Thus SCDRs and SCISRs are both surfaces of constant $\Omega(F,G)$, i.e. F = constant, if and only if the material is a purely J_2 material, i.e. $c = 0$, and then the SCISR becomes

$$\dot{\varepsilon}_{ij}^{i}\dot{\varepsilon}_{ij}^{i} = \frac{2f^{*2}(F)}{k^2}(F+1).$$

Consequently, because SCDRs are independent of the mathematical constructs of F, they are the most theoretically meaningful measurements when desiring to quantify the state dependency of the dissipation and assess the applicability of the important normality condition (i.e., convexity of this potential).

Next, consider a macromechanical viscoplastic model that describes the inelastic behavior of a unidirectional metal matrix composite which possesses transverse isotropy (Robinson and Duffy, 1990). Here the scalar function F is defined as

$$F = \frac{1}{k_T^2}\left(I_1 + \frac{1}{\eta^2}I_2 + \frac{9}{4(4\omega^2 - 1)}I_3\right) - 1 \tag{4}$$

where the following definitions apply:

4

$$I_1 = J_2 - I + \frac{1}{4}I_3, \quad I_2 = I - I_3, \quad I_3 = \left(I_0\right)^3$$
$$I = D_{ij}\Sigma_{jk}\Sigma_{ki}, \quad I_0 = D_{ij}\Sigma_{ji} \tag{5}$$
$$\eta = \frac{k_L}{k_T}, \quad \omega = \frac{Y_L}{Y_T}$$

D_{ij} is formed from the self-product of the unit vector pointing in the fiber direction, and η and ω denote the threshold stress ratios for shear and normal loading, respectively. The subscript L refers to the longitudinal direction and T the transverse direction. Similar to the isotropic material case, it can be shown that SCDRs are proportional to surfaces of constant F (i.e., Ω=constant) whereas SCISRs are not. In fact, even if we restrict the problem to a longitudinally reinforced tube subjected to only axial-torsional loading, the SCISRs are not necessarily proportional to surfaces of constant F. SCDRs and SCISRs for this case are,

$$\Sigma_{ij}\dot\varepsilon_{ij}^i = 2f^*(F)k_T^2(F+1)$$

$$\dot\varepsilon_{ij}^i\dot\varepsilon_{ij}^i = 2f^{*2}(F)\left[k_T^2(F+1) - \xi(1-\xi)\tau^2 - \frac{1}{3}\varsigma(1-\varsigma)\sigma^2\right] \tag{6}$$

$$= 2f^{*2}(F)\left[(1-\xi)^2\tau^2 + \frac{1}{3}(1-\varsigma)^2\sigma^2\right],$$

respectively, where σ denotes the axial stress component and τ the shear stress component,

$$\xi = \frac{\eta^2 - 1}{\eta^2}, \quad \varsigma = \frac{4\left(\omega^2 - 1\right)}{4\omega^2 - 1} \tag{7}$$

and F reduces to

$$F = \frac{1}{k_T^2}\left(\frac{1}{4\omega^2 - 1}\sigma^2 + \frac{1}{\eta^2}\tau^2\right). \tag{8}$$

The fact that SCISRs are not necessarily proportional to surfaces having a constant value of F is significant because the desirable convexity and normality features associated with constant F (i.e., Ω=constant) surfaces are not guaranteed for these SCISRs. Experimentally however, SCISRs have been thought to possess a distinct advantage over SCDRs for TMCs, as they can be determined from multiple probing experiments on a single specimen because only a negligibly small change in material state occurs during each probe. As will be discussed in more detail later, this may not be the case for SCDRs, where due to the anisotropy, a large inelastic strain rate must accompany the relatively low stress in the weak direction. Furthermore, stress concentrations leading to very localized inelastic deformation could conceivably preclude multi-probe SCDR or SCISR experiments on a single specimen.

With this background in mind, our objective in this paper is to analytically (using the method of cells micromechanics model) generate macro flow/damage surfaces for a representative titanium matrix composite system (i.e., SCS-6/TIMETAL 21S) and critique the resulting geometric shapes (given various definitions of these surfaces). This critique will be conducted relative to the theoretical implications when desiring to represent such macro surfaces using a macromechanics based constitutive model and the experimental implications when attempting to

experimentally measure them. It is hoped and anticipated that this work will provide insight and guidance for future experimental programs aimed at developing macro anisotropic constitutive models as well as multiaxially validating currently proposed micromechanical theories.

MICROMECHANICAL MODEL

The method of cells micromechanical model (detailed in the monograph by Aboudi, 1991) was used by Pindera and Aboudi (1988) to predict yield surfaces for MMCs. Micromechanics was also employed by Dvorak (1991) to determine yield surfaces for MMCs using a bimodal plasticity theory (Dvorak, 1987). In both of these efforts perfect bonding was assumed between the fiber and matrix. Aboudi (1989) incorporated debonding due to shear loading into the method of cells and predicted initial yield surfaces and debonding envelopes. The current work employs a more general debonding model and employs different concepts to define flow/damage surfaces.

The constitutive relations and/or parameters used to describe the fiber, matrix, fiber-matrix interface, and the overall composite are presented here. A model TMC system (SCS-6/TIMETAL 21S), having a unidirectional continuous silicon carbide (SiC) fiber reinforcement, is used throughout this paper. Additionally, given that a model material concept (Arnold and Castelli (1995)) holds, the same approach and conclusions found here should apply to other TMCs systems as well.

Silicon Carbide Fibers

Textron's high-strength, high-stiffness, continuous SiC fibers (i.e., SCS-6) are approximated as being isotropic and linear elastic. Furthermore, since the variation of elastic properties with temperature is relatively small, the following isothermal elastic properties are used throughout: Young's modulus, $E = 400$ GPa; Poisson ratio, $v = 0.25$; and coefficient of thermal expansion, $CTE = 4.5 \times 10^{-6} \, °C^{-1}$.

Titanium Matrix

The titanium alloy TIMETAL 21S® (Ti-21s) is a metastable beta strip alloy, containing approximately 21% alloying additions, that has high strength as well as good creep and oxidation resistance. Ti-21s is commonly used in advanced metal matrix composites, hence its (isotropic) viscoplastic response has been characterized for the model of Bodner and coworkers (Chan et al., 1988), Chan and Linholm, 1990)) by Kroupa and Neu (1993) as well as a generalized viscoplasticity with potential structure (GVIPS) model (Arnold and Saleeb, 1994) by Arnold et al. (1996a,b). The GVIPS model of Arnold et al. (1996a,b) has been selected for the current study. The model has one tensorial internal variable, the back stress, whose evolution includes nonlinear kinematic hardening and both thermal and strain induced recovery mechanisms. The use of a nonlinear compliance operator in the evolution law permits the flow and evolution laws to be fully associated, which greatly influences the multiaxial response under nonproportional loading (Arnold et al., (1995)).

The flow and evolution equations are, respectively,

$$\dot{\mathcal{E}}_{ij}^i = \begin{cases} 0 & \text{if } \hat{F} < 0 \\ \dfrac{3\|\dot{\mathcal{E}}_{ij}^i\|\Sigma_{ij}}{2\sqrt{J_2'}} & \text{if } \hat{F} \geq 0 \end{cases}$$

$$\dot{A}_{ij} = \begin{cases} Q_{ijmn}E_{mnkl}b_{kl} & \text{if } a_{ij}\Sigma_{ij} < 0 \\ b_{ij} & \text{if } a_{ij}\Sigma_{ij} \geq 0 \end{cases} \tag{9}$$

$$\dot{a}_{ij} = L_{ijkl}\left(\dot{A}_{kl} - \theta_{kl}\dot{T}\right),$$

where the dot represents time differentiation, A_{ij} is the deviatoric back strain tensor, a_{ij} the deviatoric back stress tensor, T is temperature, and

$$\|\dot{\mathcal{E}}_{ij}^i\| = \sqrt{\frac{2}{3}\dot{\mathcal{E}}_{ij}^i\dot{\mathcal{E}}_{ij}^i} = \frac{\mu_o \hat{F}^n}{\kappa} \quad \text{(equivalent inelastic strain rate)}$$

$$L_{ijkl} = Q_{ijkl}^{-1} = \frac{\kappa_o^2}{3B_0\left(1 + B_1 pG^{p-1}\right)}\left(\delta_{ik}\delta_{jl} - \frac{3B_1(p-1)G^{p-2}}{\kappa_o^2\left[1 + B_1 pG^{p-1}(6p-5)\right]}\right) \quad \text{(stiffness operator)}$$

$$b_{ij} = \dot{\mathcal{E}}_{ij}^i - \left(\frac{3\beta\kappa\dot{\bar{\varepsilon}}^{vp}H_v[Y]}{2\kappa_o^2\sqrt{G}} + \frac{3R_\alpha B_0 G^q}{\kappa_o^2}\right)a_{ij}$$

$$\theta_{ij} = \frac{\partial B_0}{\partial T}\left(1 + B_1 pG^{p-1}\right)\frac{3a_{ij}}{\kappa_o^2} \quad \text{(dynamic thermal recovery operator)}$$

$$\hat{F} = \left\langle \frac{\sqrt{J_2'}}{\kappa} - Y \right\rangle \quad \text{(threshold function)}$$

$$Y = \left\langle 1 - \beta\sqrt{\hat{G}} \right\rangle \quad \text{(yield stress function)}$$

$$\hat{G} = \frac{I_2'}{\kappa_o^2} \quad \text{(back stress function)}$$

$$I_2' = \frac{3}{2}a_{ij}a_{ij}, \quad J_2' = \frac{3}{2}\Sigma_{ij}\Sigma_{ij} \quad \text{(stress invariants)} \tag{10}$$

where E_{ijkl} are elastic stiffness coefficients, $H_v[\cdot]$ is the Heaviside unit step function, and $<\cdot>$ are Macauley brackets. The temperature-independent material parameters are: κ_o, n, B_1, p and q, while the temperature-dependent material parameters are: κ, μ_o, B_0, R_α, and β. Interpolation functions defined by Arnold, et al. (1996a)) are employed to determine the material parameters for Ti-21s at temperatures other than the reference temperature, 650°C. A limitation of the material characterization is that above 704°C, material parameters are taken to be those at 704°C. Material parameters at various temperatures are presented in Table 1.

Fiber-Matrix Interface

As alluded to in the introduction, fiber-matrix debonding significantly affects the stiffness and strength of TMCs. The weak interfacial bond is due to the multi-layer coating applied to the

fiber prior to consolidation. In this section, interfacial constitutive equations between tractions, T_i, and displacements, u_i, for an interface subjected to combined normal and tangential loading are summarized from Lissenden (1996). Experimental results suggest that interfacial debonding initiates upon the traction attaining a critical value - defined as the interfacial strength, T_o. For the simple case of normal separation, the interfacial strength and ductility are sufficient to characterize interfacial separation. The ductility, u_o, represents the interfacial displacement at which the traction vanishes. If, after initiation, debonding proceeds in a smooth fashion, the traction-displacement relation can be taken to be a cubic polynomial (Fig. 1):

$$\frac{T}{T_o} = 1 - 3\left(\frac{u}{u_o}\right)^2 + 2\left(\frac{u}{u_o}\right)^3 . \tag{11}$$

To generalize eq. (11) for combined normal and tangential loading, an x,n,t interface coordinate system is defined having the x-direction parallel to the fiber, n-direction normal to the interface, and t-direction tangent to the interface and orthogonal to the fiber direction. The traction and displacement components are normalized as follows:

$$\bar{u}_x = \frac{u_x}{\alpha u_o}, \quad \bar{u}_n = \frac{u_n}{u_o}, \quad \bar{u}_t = \frac{u_t}{\alpha u_o}$$
$$\bar{T}_x = \frac{T_x}{\lambda T_o}, \quad \bar{T}_n = \frac{T_n}{T_o}, \quad \bar{T}_t = \frac{T_t}{\lambda T_o} \tag{12}$$

where α defines the tangential-to-normal ductility ratio and λ defines the shear-to-normal strength ratio. In addition, a normalized Coulomb frictional traction is defined

$$\bar{T}_f = -\mu\langle -\bar{T}_n\rangle \tag{13}$$

where μ is the coefficient of static friction. A quadratic interaction of the tractions is employed to predict the initiation of debonding to occur when

$$\bar{T} = \left\{\langle \bar{T}_x - \text{sgn}(\bar{T}_x)\bar{T}_f\rangle^2 + \langle \bar{T}_n\rangle^2 + \langle \bar{T}_t - \text{sgn}(\bar{T}_t)\bar{T}_f\rangle^2\right\}^{1/2} \geq 1 \tag{14}$$

where

$$\text{sgn}(x) \equiv \begin{cases} -1 & \text{for } x < 0 \\ 1 & \text{for } x > 0 \end{cases} \tag{15}$$

and Macauley brackets are used in the normal traction term because compressive loading is not considered to be detrimental to the condition of the interface. Macauley brackets are used in the tangential traction terms to ensure that tangential interfacial displacements do not occur until after the static frictional force has been overcome.

Once debonding has initiated, the tractions can be related to the displacements by generalizing eq. (11) and including frictional effects as follows:

$$\left.\begin{aligned} \bar{T}_n &= F^*(\bar{u}_{\text{max}})\bar{u}_n, \text{ for tensile separation}\\ \bar{T}_x &= F^*(\bar{u}_{\text{max}})\bar{u}_x + \text{sgn}(\dot{\bar{u}}_x)\bar{T}_f\\ \bar{T}_t &= F^*(\bar{u}_{\text{max}})\bar{u}_t + \text{sgn}(\dot{\bar{u}}_t)\bar{T}_f \end{aligned}\right\} \text{for } 0 < \bar{u} < 1 \tag{16}$$

and

$$\left.\begin{array}{l} \overline{T}_n = 0, \text{ for tensile separation} \\ \overline{T}_x = \text{sgn}(\ddot{u}_x)\overline{T}_f \\ \overline{T}_t = \text{sgn}(\ddot{u}_t)\overline{T}_f \end{array}\right\} \text{for } \overline{u} \geq 1 \tag{17}$$

where

$$\overline{u} = \left\{\overline{u}_x^2 + \overline{u}_n^2 + \overline{u}_t^2\right\}^{1/2} \tag{18}$$

represents the normalized resultant interfacial displacement and

$$F^*(\overline{u}) = \left(1 - 3\overline{u}^2 + 2\overline{u}^3\right)\!/\overline{u} \tag{19}$$

represents the generalized form of eq. (11). The maximum value of $\overline{u} = \overline{u}_{max}$ is utilized in eq. (19) to prevent the interface from being self-repairing upon unloading. The primary difference between this model and that of Needleman (1987) and Tvergaard (1990) is the inclusion of a debond initiation criterion.

Homogenization

The method of cells (Aboudi, 1991) is a versatile micromechanical model for predicting the overall response of composites. Overall elastic properties are determined in closed-form. The microstructure is assumed to be doubly periodic, therefore it is sufficient to consider a unit cell containing a single fiber. The unit cell consists of one fiber subcell and three matrix subcells, although a recent generalization of the method permits an arbitrary number of subcells, enabling the analysis of various microstructures (Paley and Aboudi, 1992 and Aboudi, 1995). For the current work the standard version of the method of cells is adequate, the generalized method will be used in future work to study the effects of microstructure on flow/damage surfaces. Subcells are represented by rectangular geometries strictly as a mathematical convenience. The square unit cell results in a material having cubic symmetry, no attempt has been made in the current work to force the material to be transversely isotropic. Since equilibrium of tractions and compatibility of displacements are imposed at the interfaces in an average sense, the actual geometry of each subcell is only felt in a weighted average sense, i.e., the "square" fiber is really only a pseudo-square fiber as only the ratio of l/h is important.

A linear displacement field in each subcell is sufficient for determining overall response. The displacement field is continuous except at the fiber-matrix interface, where average interfacial displacement components are defined. Additionally, tractions must be continuous across subcell interfaces. It is recognized that the subcell inelastic strains are approximate, but also that the numerical efficiency of the model far exceeds that of other, perhaps more exact methods such as finite element analysis using a large number of elements.

Altogether, homogenization provides 24 equations, but there are 30 unknown variables. The fiber-matrix debonding relations presented in the previous section provide the additional six equations. McGee and Herakovich (1992) showed how to reduce the full system of equations to six with the interfacial displacements as the only unknown variables by considering different types of applied loading.

9

RESULTS

Aboudi's micromechanical model was applied to an SiC/Ti composite having a fiber volume fraction of 0.35 and the constituent properties discussed in the previous section. Residual stresses associated with processing were accounted for by cooling the composite down from a stress-free temperature of 815°C to room temperature in two hours. Subsequently, strain controlled probing tests were conducted at a relatively slow rate, 10μ/sec, to simulate the rate that might be used in an experiment. The material was in a pristine state (as processed) at the beginning of each probe and 180 probes were employed to determine each flow/damage surface. The interface properties are shown in Table 2 and were chosen to be representative of an SiC/Ti interface (Lissenden, 1996). However, in some cases the interfacial strength, T_o, has been allowed to take on different values, e.g., 100 MPa and 300 MPa.

To illustrate the marked difference in the effects of matrix inelasticity and fiber-matrix debonding, Fig. 2 shows the transverse tensile response (90°) for; (i) matrix inelasticity/perfect bonding (a continuous displacement field), (ii) an elastic matrix/debonding fiber-matrix interface, and (iii) matrix inelasticity/ debonding. Residual stresses associated with processing have been considered in all three predictions. Clearly, debonding causes a deviation from proportionality (DFP) prior to the onset of matrix inelasticity. Note that the unloading modulus (stiffness) has been degraded for the two cases in which debonding occurred. The precise representation of this unloading response, however, is relatively unimportant in the present work as only the loading portion of each probing experiment is utilized.

The stress-strain responses for axial, transverse, and axial shear loadings are shown in Fig. 3 for three temperatures of interest: 23, 300, and 500°C. Residual stresses have been considered and the (weak) interface properties shown in Table 2 were employed and assumed to be temperature-independent. While the tensile axial response is independent of fiber-matrix debonding, both the tensile transverse and shear responses are greatly affected by debonding as one would expect. In this interface model, as in others, an instability associated with the redistribution of stress from the fiber to the matrix as the interface debonds can occur, as it does for transverse tension at 300 and 500°C. No significant instability is evident at 23°C, where the interface properties were chosen to match experimental results. This suggests that more accurate results could be obtained by determining the interface properties as a function of temperature,.

Flow Surfaces for Perfect Bonding

Composite, or macro, flow surfaces of constant deviation from proportionality (SCDFPs) in transverse-axial (σ_{22}-σ_{11}), transverse-transverse (σ_{22}-σ_{33}), and shear-axial (σ_{12}-σ_{11}) stress spaces are shown in Fig. 4 for the perfect bond condition and target deviations of 10μ and 0.2% (2000 μ). The deviation from proportionality is due entirely to matrix inelasticity for perfect fiber-matrix bonding. Thus, for this case, SCDFPs are akin to yield surfaces, but in general could also be associated with internal damage. Overall SCDFPs are defined by the equivalent inelastic strain invariant, $\|\varepsilon^i\| = \sqrt{\dfrac{2}{3}\varepsilon_{ij}^i\varepsilon_{ij}^i}$, attaining a critical value; i.e., 10μ and 0.2% as in Fig. 4. The 10μ definition gives an indication of first yielding and has been shown to be significant for experimental yield surface determination (e.g., Phillips et al. (1972), Liu and Greenstreet (1976), Helling et al. (1986), Lissenden et al. (1996b)) in monolithics. Likewise, the value of 0.2% is the commonly used strain offset definition for monolithic materials and provides an indication of

10

significant plastic deformation. In reality, the 0.2% definition is frequently not applicable to reinforced materials because the reinforcing can fail prior to achieving an overall permanent strain of 0.2%, particularly for loading in the direction of the reinforcing. This however, underscores the importance of selecting an appropriate flow definition. The tensile fiber fracture envelope (for a fiber strength of 4000 MPa) is also shown in Fig. 4 to illustrate that 0.2% is not realistic for SiC/Ti-21s, nonetheless it is of academic value for comparing localized inelasticity with gross overall inelasticity.

Applying the target values of 10μ and 0.2% to our model TMC system, one can see not only a difference in size of the resulting flow (yield) surfaces depicted in Fig. 4, but in the σ_{22}-σ_{11} and σ_{22}-σ_{33} stress spaces a noticeable change in shape is also evident. Table 3 presents a comparison between the local (subcell) equivalent inelastic strains and their macroscopic (overall) counterparts at various locations on the SCDFPs of Fig. 4. For the selected points, the ratio of the maximum local equivalent inelastic strain to the value of the macroscopic SCDFP ranges from 4.1 (point E) to 6.1 (point A) and 2.4 (point D) to 3.6 (point H) for 10μ and 0.2% SCDFPs, respectively. The fact that the maximum-local-to-macroscopic equivalent inelastic strain ratio is larger for the 10μ target value than for the 0.2% case provides the proper indication that matrix inelasticity is more localized for the 10μ SCDFP. The corners appearing on the 10μ SCDFPs (Fig. 4) are associated with the change in location of the localized inelastic strain, i.e., on one side of a corner matrix inelasticity occurs in one subcell while on the other side of the corner it occurs in a different subcell. These corners are an artifact of the approximate microstructure employed by the method of cells and were also observed by Pindera and Aboudi (1988). Future work will investigate more accurate microstructural representations. Finite element analysis (Dvorak et al., 1973) has validated the overall SCDFPs obtained by the method of cells.

The implications of these results for an experimental program reside in the fact that if it is desired to limit local (constituent) equivalent nonlinear strains (so as to minimize any change in internal state) to 50μ, for example, it would be necessary to choose an overall DFP value less than 10μ in the σ_{22}-σ_{11} stress space while an overall DFP value slightly greater than 10μ could be employed in the σ_{12}-σ_{11} stress space. In either case, the in-situ, unmeasurable (using extensometry or strain gages) local, nonlinear strains would be approximately 5 times greater than their macroscopic (measurable) counterparts.

Utilizing the alternative SCDR concept to define overall flow surfaces, the predicted SCDRs from the current micro-model and surfaces of F=constant (eq. (4)) from the macro-model of Robinson and Duffy (1990) are shown in Fig. 5 for the case of no residual stresses. The strengths of anisotropy required for the macro-model were obtained by using the micro-model to simulate normal and shear loading experiments, yielding $\omega = 1.7$, $\eta = 0.83$, and $k_T = 610\,\text{MPa}$. The value of F was chosen such that the micro-predicted and macro-predicted overall surfaces agreed in the σ_{12}-σ_{11} stress space. The two overall SCDRs agree reasonably well in the σ_{22}-σ_{11} stress space, but less so in the σ_{22}-σ_{33} stress space where transverse stresses dominate. This observation is supported by Arnold et al. (1993) in related work dealing with creep-plasticity interaction wherein it was shown that non-associated models (such as Robinson and Duffy, 1990) can accurately represent longitudinal behavior and yet are inadequate for transverse stresses, while associated models of the GVIPS class (see Arnold and Saleeb, 1994, and Arnold et al., 1996a,b) provide more consistent results. It is not obvious why applying a small amount of σ_{22} causes the

dissipation rate target value to be achieved at a larger σ_{11} (Fig. 5), but this is indeed the case as was also observed by Pindera and Aboudi (1988) and Dvorak et al. (1973) for yield surfaces.

The centers of all surfaces in Fig. 5 are located at the origin because residual stresses have not yet been included. If we now account for residual stresses in the micro-model the centers of the surfaces shift as shown in Fig. 6. The residual stresses are observed to strengthen the composite under equi-biaxial transverse tension, but weaken it under equi-biaxial transverse compression (Fig. 6c). In the macro-model we attempt to account for residual stresses by equating the initial back stress to the center of the predicted micro-model surface, here $a_{11} = -241$ MPa. The comparison shown in Fig. 6 indicates that this is a viable macro-modelling technique to account for a material having different flow stresses in tension and compression.

Applied loading (strain) rate can greatly affect flow behavior, particularly at elevated temperatures. The SCDFPs shown in Fig. 7 for loading rates of 2, 20, 200, and 800 μ/sec at 500°C illustrate the rate dependency that one would expect for such a surface (here one should not think of a yield surface, but rather a surface of constant inelastic strain). Since inelastic deformation takes time to occur, more inelasticity will result from slower loading rates. On the other hand, SCDRs (and SCISRS) depend on the inelastic strain *rate* and thus are affected quite differently by loading rate. SCDRs are observed to decrease in size, and change shape, as the loading rate is increased. Furthermore, the loading rate is an upper bound on the inelastic strain rate and if the loading rate is too slow (e.g., 25 μ/sec in Fig. 7b) it may not be possible to determine an entire SCDR. As will be discussed subsequently, a discontinuity in the inelastic strain rate occurs at the threshold stress due to the formulation of the viscoplastic material model. Once the loading rate gets fast enough, this discontinuity will cause the target dissipation rate value to be exceeded at the threshold stress, which explains why SCDRs for 1000 μ/sec and 10000 μ/sec are essentially the same and suggests that for extremely fast loading rates SCDRs are rate-independent.

Flow/Damage Surfaces

Damage envelopes for metal matrix composites have previously been predicted by Aboudi (1989). Here, the concept of a damage envelope has been combined with that of a yield or flow surface resulting in SCDFPs (rate-independent) or SCDRs and SCISRs (rate-dependent). In the current work we are defining damage to be fiber-matrix debonding, other forms of damage such as matrix cracking, fiber breakage, and void growth are specifically excluded. The effects of local events (i.e., debond initiation and subcell stresses attaining their threshold value, $\hat{F} \neq 0$) on overall SCDFPs are shown in Fig. 8 by superimposing damage initiation (eq. (14)) envelopes and matrix threshold (eq. (10)) loci on overall 10μ SCDFPs in transverse-axial (σ_{22}-σ_{11}), transverse-transverse (σ_{22}-σ_{33}), and shear-axial (σ_{12}-σ_{11}) stress spaces at 23°C. Be aware that the initiation of debonding gives no indication of how the interfacial displacements accrue. It is clear from Fig. 8, however, that axial loading and compressive biaxial transverse loading do not initiate debonding. (As will be shown later, axial compression can lead to debonding associated with Poisson expansion.) The lower extreme of the debonding envelope in the σ_{22}-σ_{11} stress space (Fig. 8b) is associated with overall (macro) Poisson expansion due to compressive transverse applied stresses. Here, for an interfacial strength of 200 MPa, the DFP target value is attained prior to the matrix threshold when debonding occurs due to transverse loading but not due to shear loading, thereby once again suggesting that debonding affects the transverse tensile

12

response more than it does the shear response, as one might expect. Thus, the overall flow/damage SCDFP is essentially bimodal for normal loadings, in that it is the intersection of the debonding envelope and matrix threshold. However, in the presence of shear loading, an interaction between debonding and matrix inelasticity lead to deviation from proportionality.

The effect of temperature on 10μ SCDFPs is illustrated in Fig. 9 where flow/damage surfaces have been predicted for 23, 300, and 500°C. As expected, in all three stress spaces the size of the SCDFP decreases with increasing isothermal conditions and, as the interface properties were taken to be temperature-independent, the only effect temperature has on the initiation of debonding is in the magnitude of residual stresses produced (as these stresses ,which serve to clamp the interface together, relax as the temperature increases). As depicted in Fig. 3, the predicted deviation from proportionality associated with debonding occurs within a relatively small range of transverse and shear stresses.

Similarly, Fig. 10 shows how interfacial strength affects SCDFPs at 23°C. In addition to SCDFPs for interfacial strengths of 100, 200, and 300 MPa, the perfect bond condition is also shown. In σ_{22}-σ_{11} stress space (Fig. 10b), debonding due to Poisson expansion affects the SCDFP for compressive axial and transverse stresses in the case of an interfacial strength of 100 MPa, but not for higher interfacial strengths. As the interfacial strength of the composite is increased, the size of the SCDFP increases in the region where debonding has an influence with the perfect bond condition as the extreme (Fig. 10).

The effect of interface ductility, u_o, was also studied, but found to have a relatively small effect on the size and shape of the flow/damage surfaces. This was expected, since interface ductility only affects the rate at which stresses are redistributed from the fiber to the matrix upon debonding. In the σ_{22}-σ_{11} and σ_{33}-σ_{22} stress spaces, inelasticity is observed almost immediately after debond initiation and only an unrealistically high ductility would impact the inelastic surfaces. Greater interface ductility did result in slightly larger inelastic surfaces in the σ_{12}-σ_{11} stress space (not shown).

Now consider the construction of rate-dependent SCDRs and SCISRs at 500°C (Fig. 11 and 13). Both types of surfaces depend on the overall inelastic (including debonding effects) strain rate. Here it was found that the applied strain rate of 10μ/sec was too slow, in that it placed an upper bound on the inelastic strain rate and severely limited the range of values that could be used for complete SCDR and SCISR determinations. Thus, the applied probing strain rate was increased to 100μ/sec for all subsequent results. With respect to SCDRs, three target values, i.e., 1, 20, and 35 Pa/sec, are shown in three stress spaces at 500°C in Fig. 11. As with SCDFPs, SCDRs exhibit straight segments where fiber-matrix debonding dominates and fairly sharp corners at the intersection of regions dominated by matrix inelasticity and those dominated by debonding.

It is important to note that these fairly geometrically complex macro SCDRs, were predicted from a micro-model having relatively simple constituent constitutive relations (i.e., a J_2 viscoplasticity theory for the matrix and a simple multiaxial interface model). Conversely, the required mathematical form of a macro-model would have to be quite sophisticated to obtain the predicted SCDR representations shown in Fig. 11. The primary difficulty in modelling TMCs at the macroscale would appear to be in properly accounting for strain and stress localizations and the differences in tension and compression associated with damage.

Even if viable mathematical constructs for the dissipation potential can be shown to acurately predict deformation, there is still a question whether a macro-model can be used for failure and life prediction because these are known to depend on local events. However, with a micro-model we can examine local behavior. Consequently, we show the local equivalent inelastic strains corresponding to locations marked A-M on Fig. 11b and N-S on Fig. 11a tabulated in Table 4. The local equivalent inelastic strains are observed to vary greatly with loading and location. Transverse compression (points J, K, and L, Fig. 11b) creates the largest localized inelastic strains shown in Table 4; 47μ, 1280μ, and 2490μ for 1, 20, and 35 Pa/sec, respectively. The largest local-to-macro inelastic strain ratio is 4.7 and occurs for the 1 Pa/sec SCDR under transverse compression. The minimum subcell inelastic strain for each surface was zero. For transverse tension (points D, E, and F in Fig. 11b and Table 4) the macro inelastic strain is quite large due to debonding, while the local inelastic strains are either zero or relatively small.

It is known that the overall inelastic strain rate, and hence the dissipation rate, has a discontinuity associated with the initiation of debonding (as well as when the matrix threshold stress is attained), this discontinuity is shown in Fig. 12 for points E and M on the 20 Pa/sec SCDR. Also shown in Fig. 12 is the increase in the overall (macro) J_2 with the applied strain ε_{22}, clearly the values of J_2 are much larger at point M than at point E due to the presence of an axial stress. The concavity in the 20 Pa/sec SCDR at point E in Fig. 11b is associated with the redistribution of fiber stresses to the matrix upon debonding, as such it is an artifact of the type of interface model employed and consequently should not be alarming.

Inelastic surfaces can be determined experimentally at elevated temperature by applying axial-torsional loading to a thin-walled tubular specimen. It is desirable to determine an entire inelastic surface using a single specimen to avoid specimen-to-specimen scatter in results and make the program economically feasible. This requires absolutely minimizing the amount of inelastic deformation that occurs in each probe of the surface as any theory would require that these tests be performed at a fixed inelastic state of the material. Tests have been successfully conducted for target values of up to 100μ of permanent strain in each probe direction for monolithic materials containing no internal damage (e.g., Battiste and Ball, 1988). Consequently, in composite testing we must be aware of both the expected macro and micro inelastic strain fields developed during a given probe. As a result, we have tabulated in Table 4 the predicted local equivalent inelastic strains that accompany the SCDRs in the σ_{12}-σ_{11} stress space for points N-S denoted in Fig. 11a. For the applied strain rate of 100μ/sec it appears feasible to experimentally determine a 1 Pa/sec SCDR on a single specimen as both the local and macro equivalent inelastic strains should be relatively small at points N and Q. However, it may not be possible to experimentally determine a complete 1 Pa/sec SCDR on a single specimen because of a change in material state associated with overshooting the target value that would be likely to occur due to the relatively large (predicted) discontinuity in the dissipation rate (e.g., 10-15 Pa/sec shown in Fig. 12) associated with the initiation of debonding. Further, there is a wide disparity in macroscopic equivalent inelastic strain for shear and axial compressive loading given a value of dissipation rate. The ratio of macro equivalent inelastic strain between shear and axial compression for SCDRs of 1, 20, and 35 Pa/sec is 4.5 (N/Q), 9.5 (O/R), and 18.6 (P/S), respectively (Table 4). This wide range of equivalent inelastic strains could preclude the use of a single specimen to experimentally determine SCDRs, especially for relatively large dissipation rate target values. It should also be reaffirmed that the inelastic strain rate, and thus SCDRs and SCISRs, is very sensitive to the loading rate due to matrix viscoplasticity.

14

The shapes of the SCDRs in the three stress spaces (Fig. 11) indicate that axial-torsional tests on longitudinally reinforced thin-walled tubular specimens are not the most discriminating tests for validating the mathematical construction of the dissipation potential. Axial-transverse load probing experiments conducted on an in-plane biaxial test machine, (while being more difficult to conduct due to stress and strain gradients in the plane of the plate, coupling between axial and transverse strains, and the large potential for buckling in compression), would provide more discriminating and valuable information for the construction and validation of the mathematical representation of the dissipation potential. Biaxial transverse loading, σ_{22}-σ_{33}, would also provide valuable information, although specimens would be costly and difficult to manufacture. Alternatively, circumferentially-reinforced thin walled tubes could be employed to obtain surfaces in the σ_{12}-σ_{22} stress space, and even though this stress space was not considered in the present work these surfaces are likely to have complex geometries because both shear and transverse loading result in debonding.

Figure 13 shows 1, 15 and 25 μ/sec^2 SCISRs at 500°C, again the target values were chosen to provide the largest possible range of SCISRs. SCDRs and SCISRs are quite similar for small values, 1 Pa/sec and 1 μ/sec^2, respectively, as can be seen by comparing Fig. 11 and 13. The reason for the similarity appears to be that these small values really correspond to the initiation of either debonding or matrix inelasticity, causing the difference between $\Sigma_{ij}\dot{\varepsilon}_{ij}^i$ and $\dot{\varepsilon}_{ij}^i\dot{\varepsilon}_{ij}^i$ to be small. For larger target values, the shapes of SCDRs (Fig. 11) and SCISRs (Fig. 13) become quite different in all three stress spaces, particularly the σ_{22}-σ_{33} stress space. It should be pointed out that since $\Sigma_{ij}\dot{\varepsilon}_{ij}^i$ and $\dot{\varepsilon}_{ij}^i\dot{\varepsilon}_{ij}^i$ are different quantities, one should not expect a one-to-one correspondence between SCDRs and SCISRs. However, the values for SCDRs and SCISRs plotted in Fig. 11 and 13 were chosen to provide the widest possible range for the given loading rate and temperature, facilitating comparisons of trends between SCDRs and SCISRs for small, medium and large amounts of inelasticity. It is apparent that SCISRs are more affected by debonding than are SCDRs. This could be related to the discontinuity in the inelastic strain rate associated with the initiation of debonding. For a SCDR the discontinuous $\dot{\varepsilon}_{ij}^i$ is multiplied by the effective stress Σ_{ij}, while for a SCISR the discontinuity is magnified by multiplying $\dot{\varepsilon}_{ij}^i$ by itself.

Local and macro equivalent inelastic strains associated with the SCISRs shown in Fig. 13 are presented in Table 5. Typically, both the local and macro equivalent inelastic strains are lower for SCISRs than for SCDRs. In some cases the macro equivalent inelastic strain is considerably smaller for SCISRs than for SCDRs (transverse tension and shear). However, even for SCISRs the local equivalent inelastic strains can be quite high in some cases (axial tension/compression), having significant implications for experimental programs.

CONCLUSIONS

In this study we have generated macro flow/damage surfaces using three distinct definitions for these surfaces, i.e., "yield" (deviation from proportionality), surfaces of constant inelastic strain rate (SCISRs), and surfaces of constant dissipation rate (SCDRs). These surfaces have been calculated using the method of cells micromechanics model for a representative silicon carbide/titanium metal matrix composite (i.e., SCS-6/TIMETAL 21S) at temperatures ranging

15

from 23 to 500°C. The micromechanical analysis explicitly accounts for matrix viscoplasticity, fiber-matrix debonding, and residual stresses. The main conclusions of this study are listed here.

- The various macro flow/damage surfaces possess differences in tension and compression with their centers being offset from the origins as a result of the presence of internal (microscale) residual stress fields.
- The shape of these surfaces are distinctly affected by the presence of internal damage (i.e., fiber-matrix debonding) as well as the applied biaxial stress state.
- The size of surfaces of constant deviation from proportionality (SCDFPs) and SCISRs is decreased by debonding for transverse tension and shear loadings, distorting the shape of the inelastic surface. SCDRs are also affected by debonding, but to a lesser extent.
- The range of possible values for SCDRs determined by various applied loadings is limited by the disparity in stress magnitudes at the onset of inelasticity. This disparity in stress magnitude is attributed to the presence of fiber induced anisotropy and fiber-matrix debonding.
- Clearly axial/torsion tests are not the most discriminating tests for differentiating between surface definitions or illustrating the required mathematical constructs of the dissipation potential. Here, in-plane biaxial tests appear to be the more important and informative tests to conduct.
- The magnitude of the pertinent macro target value significantly influences the magnitude of the resulting internal state (i.e., the magnitude of local inelastic strain and internal stress) and consequently the reusability of a single test specimen for multiple surface probes.
- Given a macroscale starting viewpoint, relatively sophisticated mathematical representations (in the form of the invariants employed, the inclusion of J_3, and possibly I_1, etc.) for the macro dissipation potential would be required to capture the complex geometric properties of the various flow/damage surfaces. In contrast, employing a micromechanics model, such as the method of cells, one can use a relatively simple constituent constitutive (e.g., J_2 viscoplastic theory for the matrix) relation to obtain the required macro multiaxial behavior.
- Fiber-matrix debonding is independent of axial loading, except possibly in the case of axial compression, where debonding could occur due to transverse Poisson expansion.
- A key parameter in the ability to determine the entire SCDR accurately is the applied strain rate.

The results of this study are in agreement with those from previous macro- and micromechanics studies relating to yield and flow surfaces for metal matrix composites exhibiting perfect bonding. Here we have included fiber-matrix debonding and paid particular attention to different target values as well as different definitions of overall flow/damage. Additionally, the micromechanics model has permitted us to compare overall and local stress and strain fields as well as provide guidance for an experimental program aimed at validating multiaxial constitutive relations for metal matrix composites.

16

REFERENCES

Aboudi, J., 1989, "Micromechanical analysis of fibrous composites with Coulomb frictional slippage between the phases," *Mechanics of Materials*, Vol. 8, pp. 103-115.

Aboudi, J., 1991, *Mechanics of Composite Materials a Unified Micromechanical Approach*, Elsevier, Amsterdam.

Aboudi, J., 1995, "Micromechanical analysis of thermo-inelastic multiphase short-fiber composites", *Composites Engineering*, Vol. 5, No. 7, pp. 839-850.

Arnold, S.M. and Castelli, M.G., 1995, "What constitutes a model material?" HITEMP Review 1995, Volume II: Compressor/Turbine Materials, NASA CP-10178, pp. 35A:1-18.

Arnold, S.M. and Saleeb, A.F., 1994, "On the thermodynamic framework of generalized coupled thermoelastic-viscoplastic-damage modeling," *International Journal of Plasticity*, Vol. 10 No. 3, pp. 263-278, Also NASA TM-105349, 1991.

Arnold, S.M., Saleeb, A.F., and Wilt T.E., 1995, "A modeling investigation of thermal and strain induced recovery and nonlinear hardening in potential based viscoplasticity," *Journal of Engineering Materials and Technology*, Vol. 117, pp. 157-167. Also NASA TM-106122, 1993.

Arnold, S.M., Wilt T.E., Saleeb, A.F., and Castelli, M.G., 1993, "An investigation of macro and micromechanical approaches for a model MMC system," HITEMP Review 1993, Volume II: Compressor/Turbine Materials, NASA CP-19117, pp. 52:1-12.

Arnold, S.M., Saleeb, A.F., and Castelli, M.G., 1996a "A fully associative, nonisothermal, nonlinear kinematic, unified viscoplastic model for titanium alloys," *Thermo-Mechanical Fatigue Behavior of Materials: Second Volume, ASTM STP-1263*, M. Verrilli and M. G. Castelli, Eds. Also NASA TM-106926, 1995.

Arnold, S.M., Saleeb, A.F., and Castelli, M.G., 1996b, "A fully associative, nonlinear kinematic, unified viscoplastic model for titanium alloys," *Life Prediction Methodology for Titanium Matrix Composites, ASTM STP-1253*, W.S. Johnson, J.M. Larsen, and B.N. Cox, Eds. Also NASA TM-106609, 1995.

Battiste, R. L. and Ball, S. J., 1986, "Determination of surfaces of constant inelastic strain rate at elevated temperatures," *Turbine Engine Hot Section Technology*, NASA CP-2444, NASA Lewis Research Center, Cleveland, OH, pp. 307-325.

Bodner, S.R., 1987, "Review of a unified elastic-viscoplastic theory," *Unified Constitutive Equations for Creep and Plasticity*, A.K. Miller, ed., Elsevier, Amsterdam, pp. 273-301.

Chan, K.S., Bodner, S.R., and Lindholm, U.S., 1988, "Phenomenological modeling of hardening and thermal recovery in metals," *Journal of Engineering Materials and Technology*, Vol. 110, pp. 1-8.

Chan, K.S. and Lindholm, U.S., 1990, "Inelastic deformation under nonisothermal loading," *Journal of Engineering Materials and Technology*, Vol. 112, pp. 15-25.

Clinard, J.A. and Lacombe, C., 1988, "Determination of multiaxial flow surfaces at elevated temperatures using the concept of dissipation potential", Oak Ridge National Laboratory, ORNL TM-10787.

Dvorak, G.J., Rao, M.S.M, and Tarn, J.Q., "Yielding in unidirectional composites under external loads and temperature changes," *Journal of Composite Materials*, Vol. 7, pp. 194--216.

Dvorak, G.J., 1987, "Bimodal theory of fibrous composite materials," *Acta Mechanica*, Vol. 69, pp. 219-24.

17

Dvorak, G.J., 1991, "Plasticity theories for fibrous composite materials," *Metal Matrix Composites: Mechanisms and Properties*, Everett, R.K. and Arsenault, R.J., eds. Academic Press, Boston, pp. 1-77.

Ellis, J. R., Robinson, D.N., and Pugh, C.E., 1978, "Behavior of annealed type 316 stainless steel under monotonic and cyclic loading at room temperature", *Journal of Nuclear Engineering and Design*, Vol. 47, pp. 115-123.

Freed, A.D. and Walker, K.P., 1995, "Viscoplastic model development with an eye toward characterization," *Journal of Engineering Materials and Technology*, Vol. 117, pp. 8-13.

Helling, D.E., Miller, A.K., and Stout, M.G., 1986, "An experimental investigation of the yield loci of 1100-0 aluminum, 70:30 brass, and an overaged 2024 aluminum alloy after various prestrains," *Journal of Engineering Materials and Technology*, Vol. 108, pp. 313-320.

Helling, D.E. and Miller, A.K., 1987, "The incorporation of yield surface distortion into a unified constitutive model, Part 1: equation development," *Acta Mechanica*, Vol. 69, pp. 9-23.

Hopkins S.E., 1990, "A unified multiaxial J_2, J_3 theory of viscoplasticity for high-temperature isotropic materials", Masters Thesis, University of Akron, OH.

Jansson, S., Deve, H.E., and Evans, A.G., 1991, "The anisotropic mechanical properties of a Ti matrix composite reinforced with SiC fibers," *Metallurgical Transactions*, Vol. 22A, pp. 2975-2984.

Johnson, W.S., Lubowinski, S.J., and Highsmith, A.L., 1990, "Mechanical characterization of unnotched SCS_6/Ti-15-3 metal matrix composites at room temperature," *Thermal and Mechanical Behavior of Metal Matrix and Ceramic Matrix Composites, ASTM STP 1080*, Kennedy, J.M. et al., eds., American Society for Testing and Materials, Philadelphia, pp. 193-218.

Kroupa, J.L. and Neu, R.W., 1993, "Implementation of a nonisothermal unified inelastic-strain theory in ADINA6.0 for a titanium alloy - user guide," Wright Laboratory WL-TR-93-4005.

Lerch, B.A., and Saltsman, J.F., 1993, "Tensile deformation damage in SiC/Ti-15-3 laminates," *Composite Materials: Fatigue and Fracture, Fourth Volume, ASTM STP 1156*, Stinchcomb, W.W. and Ashbaugh, N.E., eds., American Society for Testing and Materials, Philadelphia, pp. 161-175.

Lissenden, C.J., Lerch, B.A., and Herakovich, C.T., 1996a, "Response of SiC/Ti under combined loading - part III: microstructural evaluation," *Journal of Composite Materials*, Vol. 30, pp. 84-108.

Lissenden, C.J., Lerch, B.A., Ellis, J.R., and Robinson, D.N., 1996b, "Verification of experimental techniques for flow surface determination," NASA TM-107053.

Lissenden, C.J., 1996, "Fiber-matrix interfacial constitutive relations for viscoplastic composites," submitted.

Liu, K.C. and Greenstreet, W.L., 1976, "Experimental studies to examine elastic-plastic behavior of metal alloys used in nuclear structures," *Constitutive Equations in Viscoplasticity: Computational and Engineering Aspects, AMD-Vol. 20*, American Society of Mechanical Engineers, New York, pp. 35-56.

Majumdar, B.S. and Newaz, G.M., 1992, "Inelastic deformation of metal matrix composites: plasticity and damage mechanisms," *Philosophical Magazine*, Vol. A66, pp. 187-212.

McGee, J.D. and Herakovich, C.T., 1992, "Micromechanics of fiber/matrix debonding," University of Virginia Report AM-92-01.

18

Needleman, A., 1987, "A continuum model for void nucleation by inclusion debonding," *Journal of Applied Mechanics*, Vol. 54, pp. 525-531.

Oytana, C., Delobelle, P., and Mermet, A., 1982, "Constitutive equations study in biaxial stress experiments", *Journal of Engineering Materials and Technology*, Vol. 104, pp. 1-11.

Paley, M. and Aboudi, J., 1992, "Micromechanical Analysis of Composites by the Generalized Cells Model", Mechanics of Materials, Vol. 14, pp. 127-139.

Phillips, A., 1974, "The Foundations of Thermoplasticity-Experiment and Theory," Topics in Applied Continuum Mechanics, J.L. Zemen and F. Ziegler (Eds.), Springer Verlag, Wien-New York, pp. 1-21.

Phillips, A., Liu, C.S., Justusson, J.W., 1972, "An experimental investigation of yield surfaces at elevated temperature," *Acta Mechanica*, Vol. 14, pp. 119-146.

Pindera, M.J. and Aboudi, J., 1988, "Micromechanical analysis of yielding of metal matrix composites," *International Journal of Plasticity*, Vol. 4, pp. 195-214.

Robinson, D.N., 1985, "On Thermomechanical Testing in Support of Constitutive Equation Development for High-Temperature Alloys", NASA CR-174879, NASA Lewis Research Center, Cleveland, OH.

Robinson, D.N. and Ellis J.R., 1986, "A multiaxial theory of viscoplasticity for isotropic materials," Turbine Engine Hot Section Technology, NASA CP-2444, NASA Lewis Research Center, Cleveland, OH, pp. 283-292.

Robinson, D.N. and Duffy, S.F., 1990, "Continuum deformation theory for high-temperature metallic composites," *ASCE Journal of Engineering Mechanics*, Vol. 116, pp. 832-844.

Saleeb, A.F. and Wilt, T.E., 1993, "Analysis of the Anisotropic Viscoplastic-Damage Response of Composite Laminates- Continuum Basis and Computational Algorithms", *International Journal of Numerical Methods in Engineering*, Vol. 36, pp. 1629-1660.

Spencer, A.J.M. , 1972, *Deformations of Fiber-Reinforced Materials*, Clarendon Press, Oxford.

Tvergaard, V., 1990, "Effect of fibre debonding in a whisker-reinforced metal," *Materials Science and Engineering*, Vol. A125, pp. 203-213.

Walker, K.P., 1981, "Research and development program for nonlinear structural modeling with advanced time-temperature dependent constitutive relationships," NASA CR-165533.

TABLE 1: Ti-21s MATERIAL PARAMETERS

	23°C	300°C	500°C	650°C	704°C
E (GPa)	114.1	107.9	95.1	80.7	59.7
CTE ($\mu°C^{-1}$)	7.717	9.209	10.70	12.13	14.09
κ (MPa)	1029	768.4	254.2	5.861	0.756
μ (MPa/sec)	667.6	137.8	1.45×10^{-3}	6.19×10^{-9}	1.13×10^{-11}
B_0 (MPa)	6.908×10^{-5}	1.035×10^{-4}	2.756×10^{-4}	5.870×10^{-4}	6.346×10^{-4}
R_α (1/sec)	0	0	1.68×10^{-7}	1.00×10^{-6}	6.01×10^{-5}
β	0.001	0	0	0	0

temperature-independent: $\nu = 0.365$, $n = 3.3$, $B_1 = 0.05$, $p = 1.8$, $q = 1.35$

TABLE 2: INTERFACE PROPERTIES

T_o (MPa)	u_o (μm)	η	α	μ
200	9	1	8	0.4

(11) (12)
(21) (22)

x_2 x_1 x_3
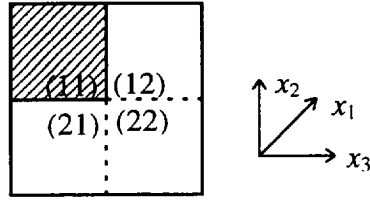
TABLE 3: MATRIX EQUIVALENT INELASTIC STRAINS ASSOCIATED WITH SCDFPs SHOWN IN FIGURE 4

Location (see Fig. 4)	subcell 12 ($\times 10^{-6}$)	subcell 21 ($\times 10^{-6}$)	subcell 22 ($\times 10^{-6}$)	maximum local/macro	DFP
A	60.8	17.7	0	6.1	10μ
B	5890	5350	5190	2.9	0.2%
C	53.7	0	0	5.4	10μ
D	4860	4460	0	2.4	0.2%
E	40.7	38.4	18.6	4.1	10μ
F	5700	5500	5380	2.8	0.2%
G	0	58.0	0	5.8	10μ
H	2150	7200	0	3.6	0.2%
I	54.5	0	0	5.4	10μ
J	4620	4700	0	2.4	0.2%
K	41.6	41.6	0	4.2	10μ
L	5670	5670	5040	2.8	0.2%
M	41.4	42.8	0	4.3	10μ
N	5630	5640	5210	2.8	0.2%
O	0	40.8	0	4.1	10 μ
P	461	6480	387	3.2	0.2%

TABLE 4: MATRIX EQUIVALENT INELASTIC STRAINS
ASSOCIATED WITH SCDRs SHOWN IN FIGURE 11

Location (see Fig. 11)	subcell 12 ($\times 10^{-6}$)	subcell21 ($\times 10^{-6}$)	subcell22 ($\times 10^{-6}$)	macro DFP ($\times 10^{-6}$)	maximum local/macro	SCDR (Pa/sec)
A	24.6	24.6	17.7	7.4	3.3	1
B	775	775	685	246	3.2	20
C	1690	1690	1540	542	3.1	35
D	0	0	0	18.5	0	1
E	1.3	0	0	1000	0.001	20
F	739	0	249	4210	0.2	35
G	16.9	16.9	14.3	5.1	3.3	1
H	618	618	574	196	3.2	20
I	1350	1350	1270	431	3.1	35
J	0	47.0	0	10.0	4.7	1
K	149	1280	11.1	307	4.2	20
L	504	2490	40.9	641	3.9	35
N	0	1.0	0	22.7	0.04	1
O	59.9	17.4	53.7	1870	0.03	20
P	4140	41.0	4020	8000	0.5	35
Q	16.9	16.9	14.3	5.1	3.3	1
R	618	618	574	196	3.2	20
S	1350	1350	1270	431	3.1	35

TABLE 5: MATRIX EQUIVALENT INELASTIC STRAINS ASSOCIATED WITH SCISRs SHOWN IN FIGURE 13

Location (see Fig. 13)	subcell 12 ($\times 10^{-6}$)	subcell 21 ($\times 10^{-6}$)	subcell 22 ($\times 10^{-6}$)	macro DFP ($\times 10^{-6}$)	maximum local/macro	SCISR (μ/sec^2)
A	14.1	14.1	9.6	4.2	3.3	1
B	606	606	530	192	3.2	15
C	1600	1600	1450	511	3.1	25
D	0	0	0	18.5	0	1
E	0	0	0	18.6	0	15
F	0	0	0	18.6	0	25
G	14.0	14.0	11.7	4.2	3.3	1
H	649	649	602	205	3.2	15
I	1740	1740	1640	555	3.1	25
J	0	14.3	0	3.0	4.8	1
K	28.4	533	1.6	120	4.4	15
L	114	1108	8.2	262	4.2	25
N	0	1.0	0	22.7	0.04	1
O	0	1.0	0	22.7	0.04	15
P	0	1.0	0	22.7	0.04	25
Q	14.0	14.0	11.7	4.2	3.3	1
R	649	649	602	205	3.2	15
S	1730	1730	1640	555	3.1	25

23
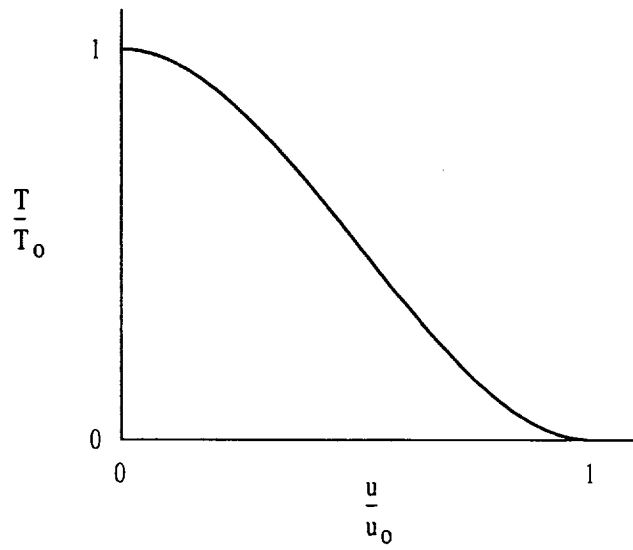
Figure 1: Traction-separation relation
for purely normal separation
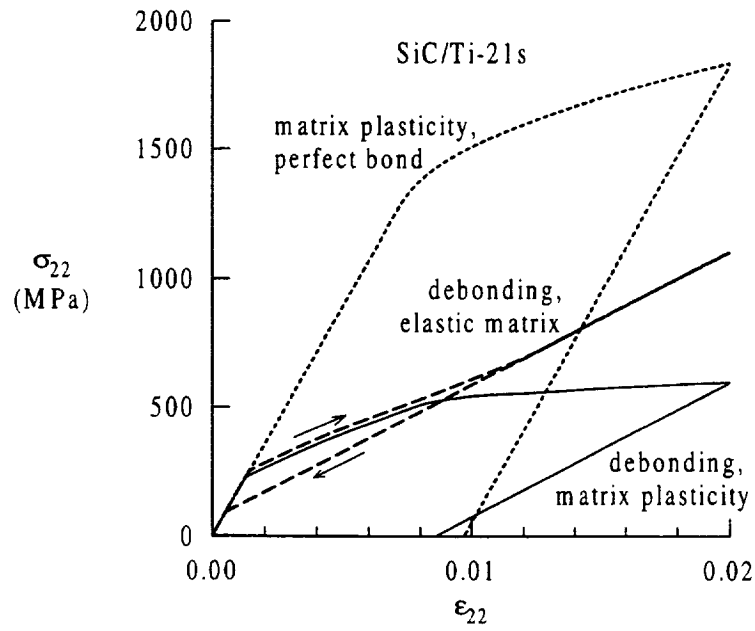
Figure 2: Comparison of matrix inelasticity and
fiber-matrix debonding

24
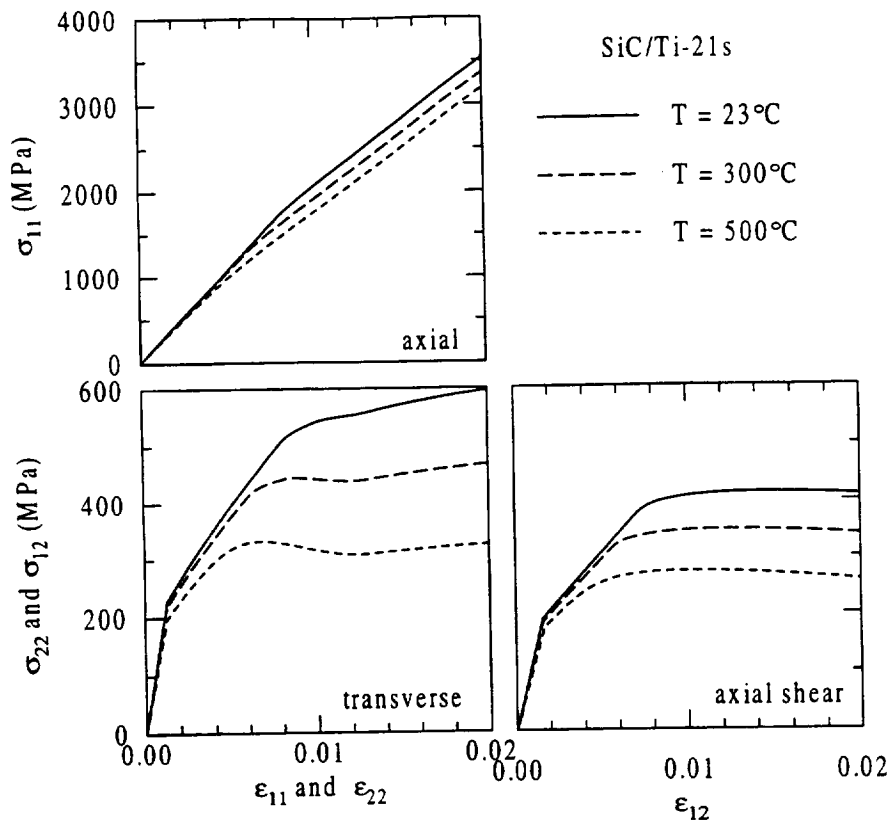
Figure 3: Stress-strain response at 23, 300, and 500°C
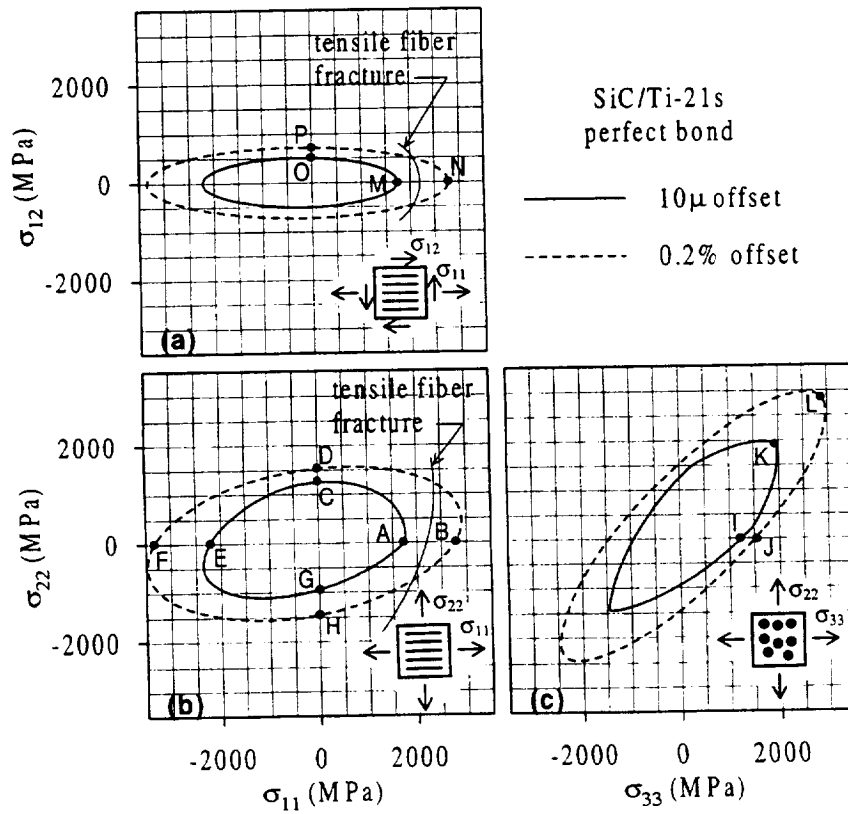
Figure 4: SCDFPs for perfect bonding at 23°C
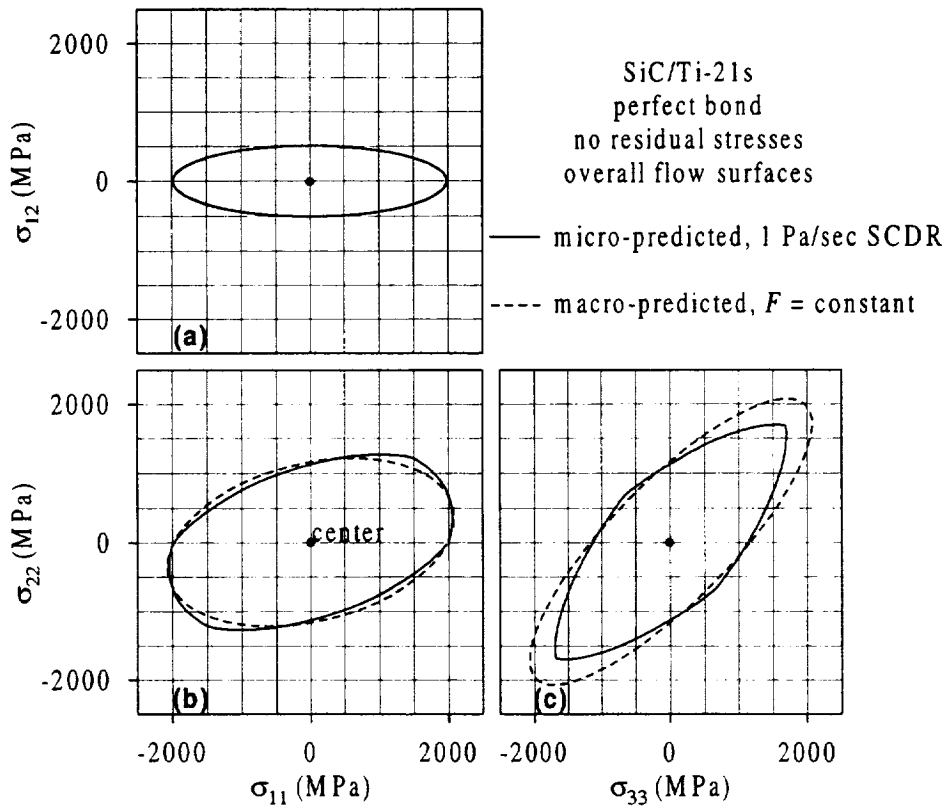
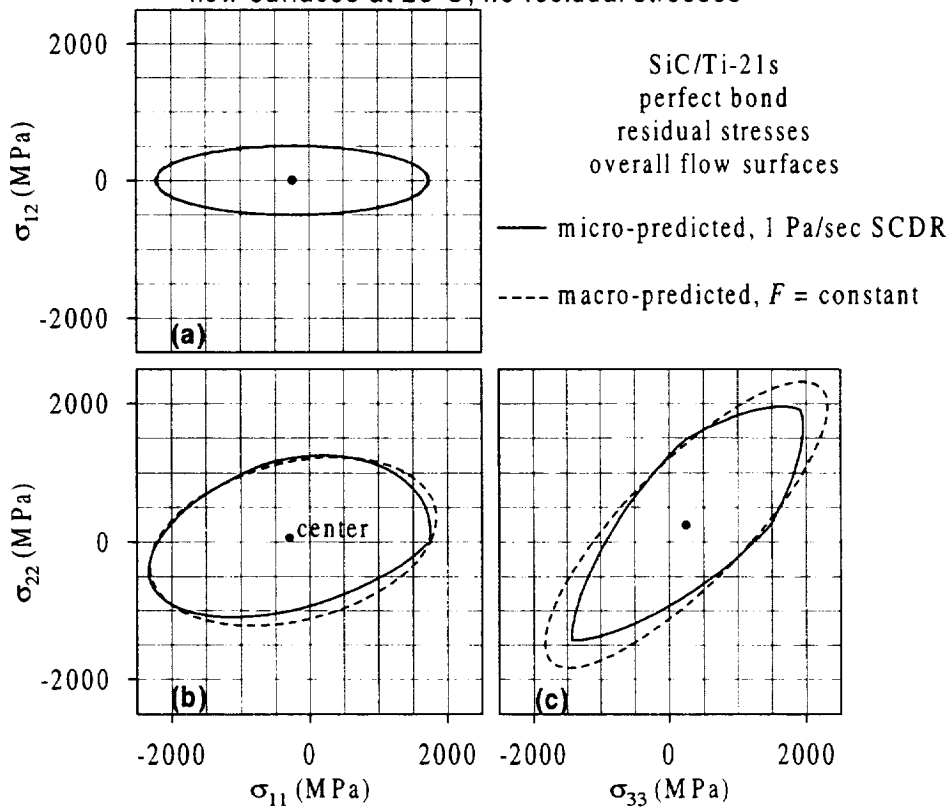Figure 5: Comparison of micro- and macro-predicted overall flow surfaces at 23°C, no residual stresses

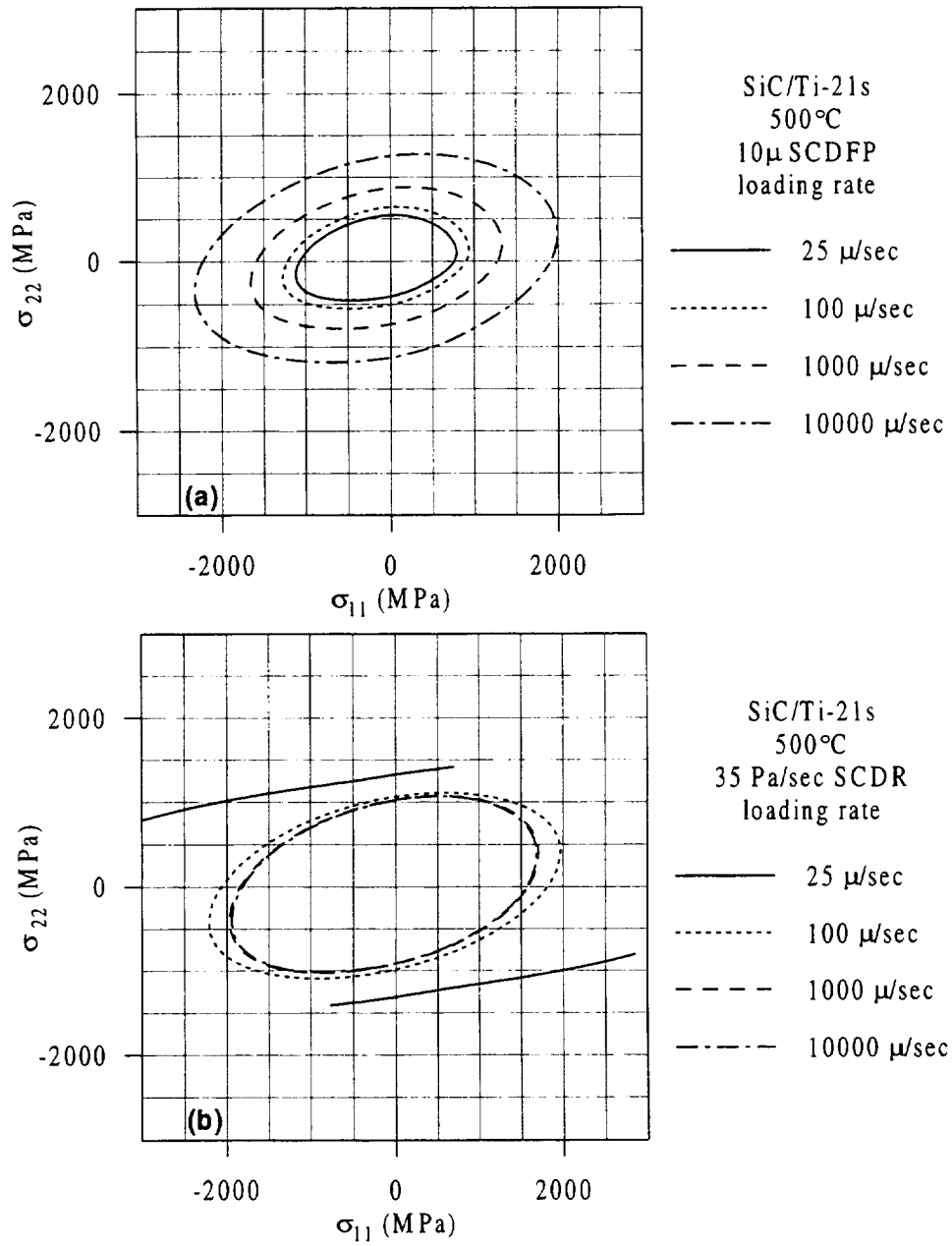Figure 6: Comparison of micro- and macro-predicted overall flow surfaces at 23°C, residual stresses included

26

(a)

σ_{22} (MPa)

2000

0

-2000

-2000   0   2000

σ_{11} (MPa)

SiC/Ti-21s
500°C
10μ SCDFP
loading rate

——————— 25 μ/sec

· · · · · · · · 100 μ/sec

– – – – 1000 μ/sec

– · – · – 10000 μ/sec

(b)

σ_{22} (MPa)

2000

0

-2000

-2000   0   2000

σ_{11} (MPa)

SiC/Ti-21s
500°C
35 Pa/sec SCDR
loading rate

——————— 25 μ/sec

· · · · · · · · 100 μ/sec

– – – – 1000 μ/sec

– · – · – 10000 μ/sec

Figure 7: Effect of loading (strain) rate on SCDFPs and SCDRs
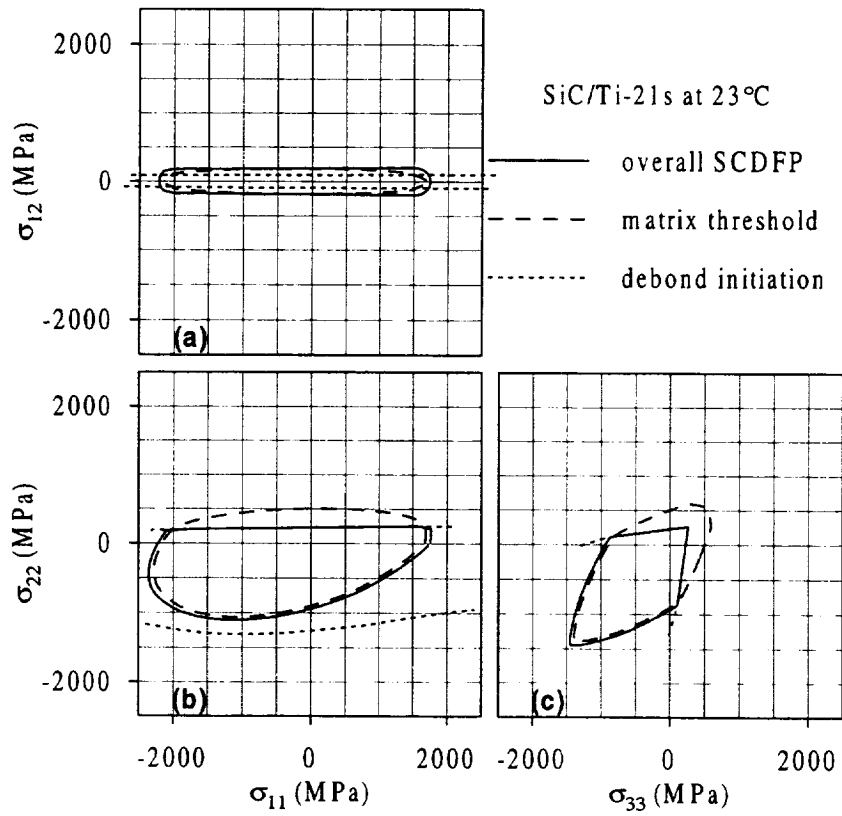
Figure 8: SCDFPs, matrix threshold, and initiation of debonding at 23 °C
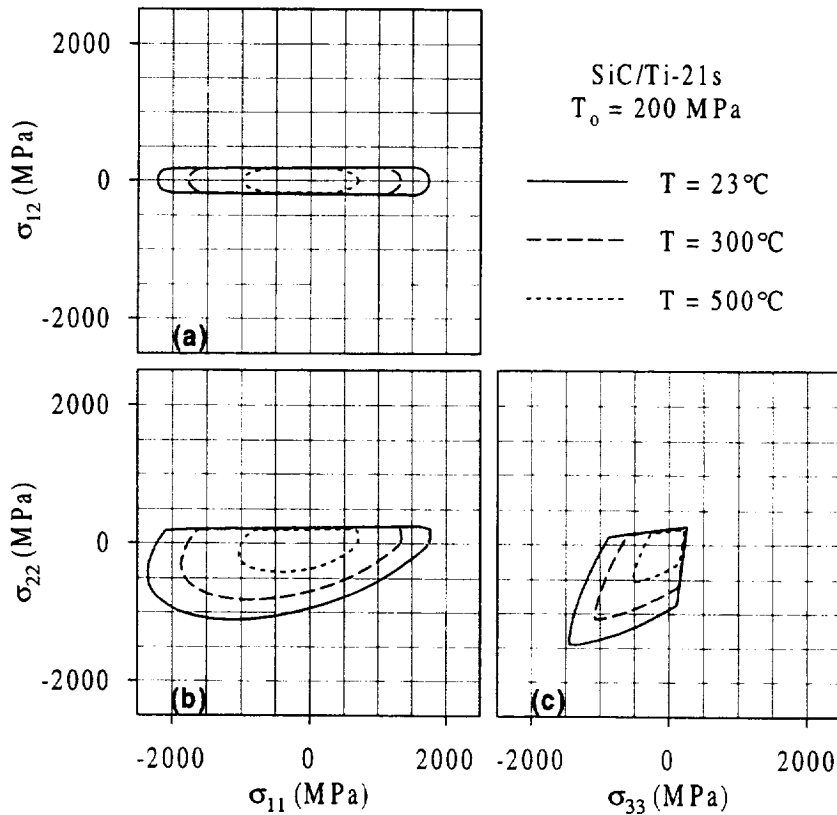
Figure 9: Effect of temperature on 10μ SCDFPs

28
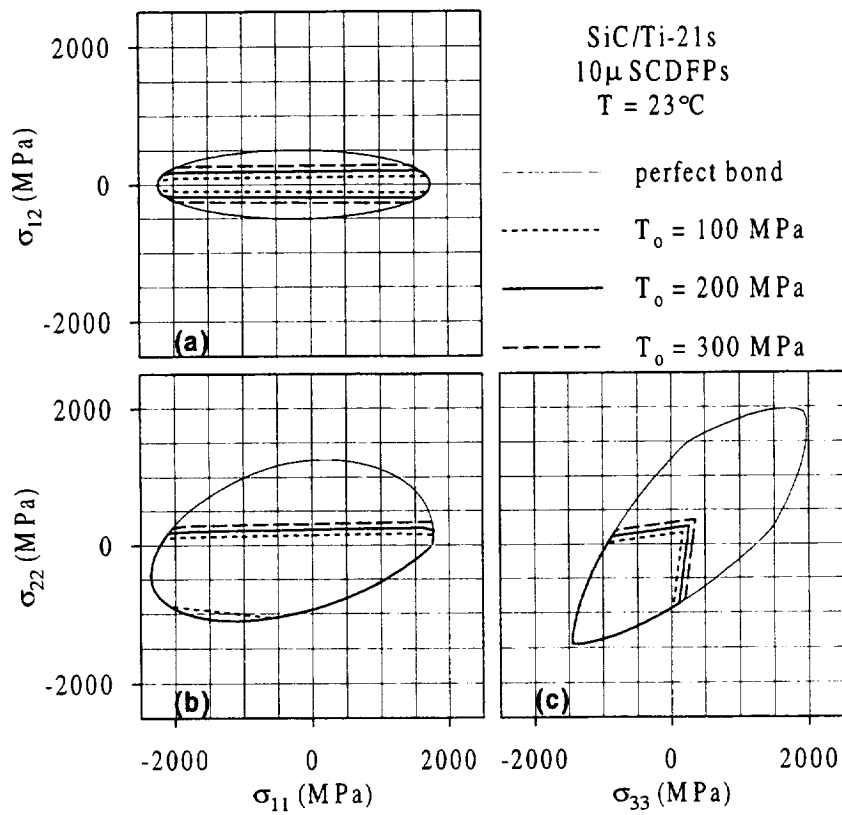
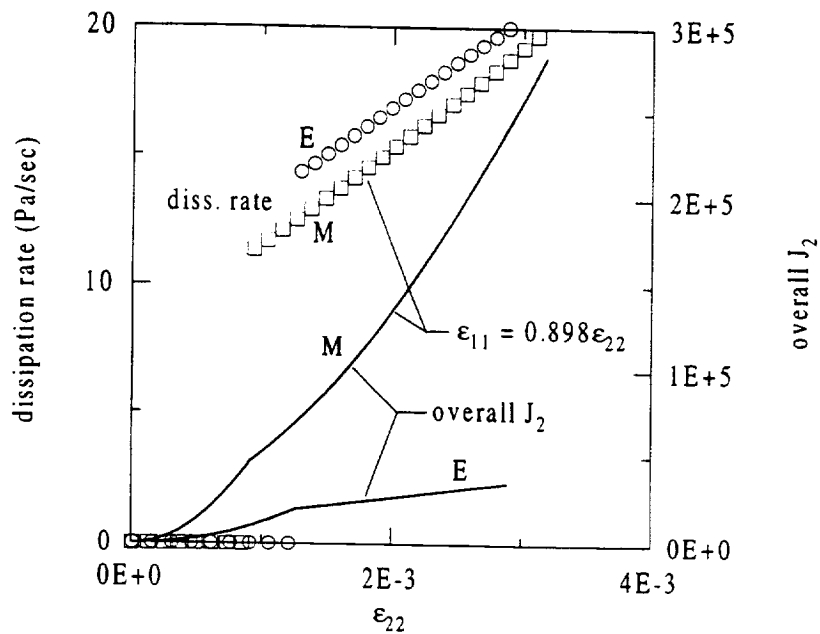Figure 10: Effect of interfacial strength on SCDFPs at 23°C
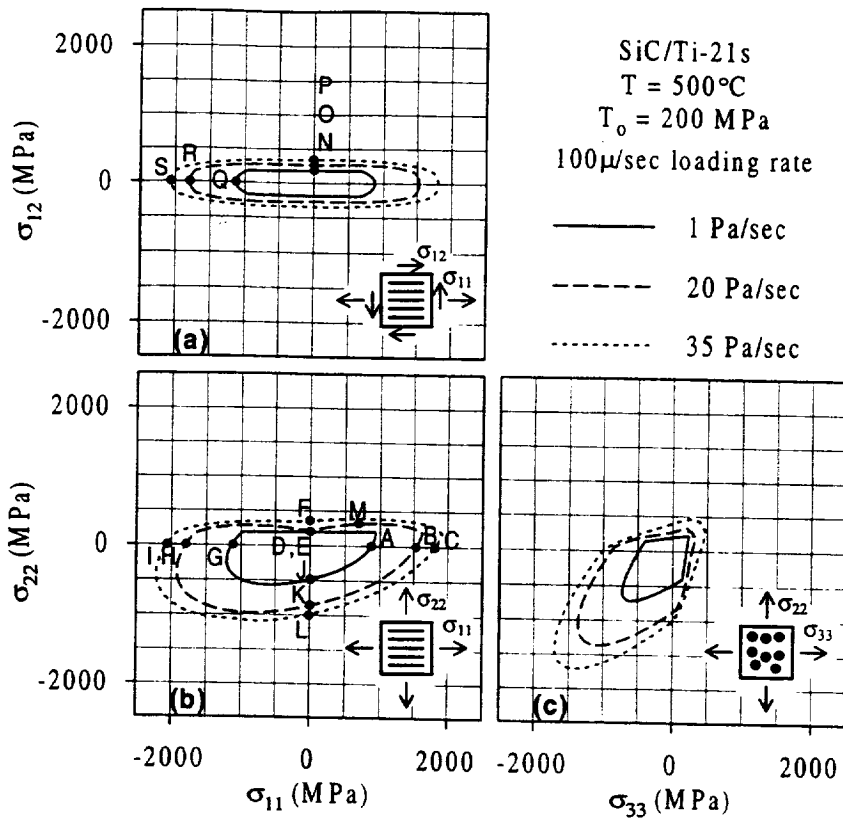
Figure 11: SCDRs at 500°C

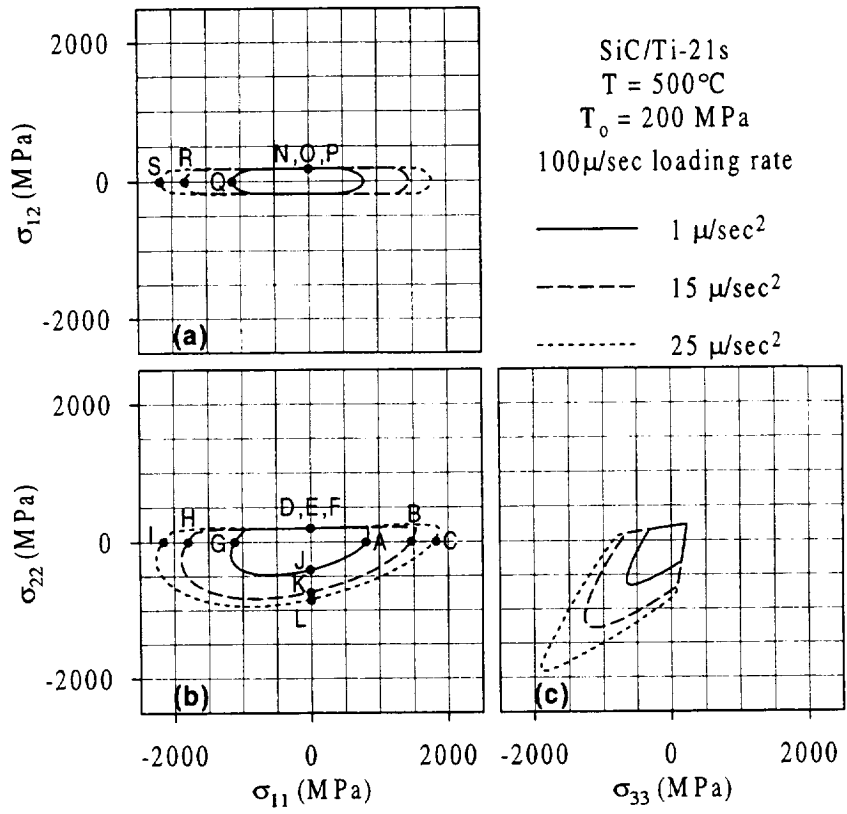Figure 12: Dissipation rate increase at points
E and M (located on Fig. 11)

Figure 13: SCISRs at 500°C

REPORT DOCUMENTATION PAGE

Public reporting burden for this collection of information is estimated to average 1 hour per response, including the time for reviewing instructions, searching existing data sources, gathering and maintaining the data needed, and completing and reviewing the collection of information. Send comments regarding this burden estimate or any other aspect of this collection of information, including suggestions for reducing this burden, to Washington Headquarters Services, Directorate for Information Operations and Reports, 1215 Jefferson Davis Highway, Suite 1204, Arlington, VA 22202-4302, and to the Office of Management and Budget, Paperwork Reduction Project (0704-0188), Washington, DC 20503.

1. AGENCY USE ONLY (Leave blank)	2. REPORT DATE	3. REPORT TYPE AND DATES COVERED
	October 1996	Technical Memorandum

4. TITLE AND SUBTITLE	5. FUNDING NUMBERS
Critique of Macro Flow/Damage Surface Representations for Metal Matrix Composites Using Micromechanics	
6. AUTHOR(S)	WU–505–63–12
Cliff J. Lissenden and Steven M. Arnold	

7. PERFORMING ORGANIZATION NAME(S) AND ADDRESS(ES)	8. PERFORMING ORGANIZATION REPORT NUMBER
National Aeronautics and Space Administration Lewis Research Center Cleveland, Ohio 44135–3191	E–10422

9. SPONSORING/MONITORING AGENCY NAME(S) AND ADDRESS(ES)	10. SPONSORING/MONITORING AGENCY REPORT NUMBER
National Aeronautics and Space Administration Washington, D.C. 20546–0001	NASA TM–107321

11. SUPPLEMENTARY NOTES

12a. DISTRIBUTION/AVAILABILITY STATEMENT	12b. DISTRIBUTION CODE
Unclassified - Unlimited Subject Categories 49 and 24 This publication is available from the NASA Center for AeroSpace Information, (301) 621–0390.	

13. ABSTRACT (Maximum 200 words)

Guidance for the formulation of robust, multiaxial, constitutive models for advanced materials is provided by addressing theoretical and experimental issues using micromechanics. The multiaxial response of metal matrix composites, depicted in terms of macro flow/damage surfaces, is predicted at room and elevated temperatures using an analytical micromechanical model that includes viscoplastic matrix response as well as fiber-matrix debonding. Macro flow/damage surfaces (i.e., debonding envelopes, matrix threshold surfaces, macro "yield" surfaces, surfaces of constant inelastic strain rate, and surfaces of constant dissipation rate) are determined for silicon carbide/titanium in three stress spaces. Residual stresses are shown to offset the centers of the flow/damage surfaces from the origin and their shape is significantly altered by debonding. The results indicate which type of flow/damage surfaces should be characterized and what loadings applied to provide the most meaningful experimental data for guiding theoretical model development and verification.

14. SUBJECT TERMS			15. NUMBER OF PAGES
Metal matrix composites; Micromechanics; Macromechanics; Viscoplasticity damage; Flow surfaces; Yield surfaces			33
			16. PRICE CODE A03

17. SECURITY CLASSIFICATION OF REPORT	18. SECURITY CLASSIFICATION OF THIS PAGE	19. SECURITY CLASSIFICATION OF ABSTRACT	20. LIMITATION OF ABSTRACT
Unclassified	Unclassified	Unclassified	